for cell survival curves. The relative biological effectiveness (RBE) for neutron beams was obtained as the ratio of the mean value of D_{10} to that of gamma rays.

Gamma-H2AX focus assay

A Gamma-H2AX focus assay was performed to detect DNA double-strand breaks (DSBs) [16]. Cells were poured onto 22 × 22 mm coverslips in 35 mm dishes filled with medium and placed in an incubator for the stated repair time after irradiation. Briefly, cells were fixed with 4% paraformaldehyde in phosphate-buffered saline (PBS), permeabilized for 10 min on ice in 0.5% Triton X-100 in PBS, washed thoroughly with PBS, and then blocked for 1 h with 3% skim milk in PBS. The coverslips were then incubated with an antibody against histone H2AX phosphorylated on serine 139 (Upstate Biotechnology, Lake Placid, NY) for 2 h at 37°C. After incubation with primary antibody, the cells were washed with PBS, and Alexa Fluor 488-labeled anti-mouse IgG secondary antibodies (Invitrogen) were added. The coverslips were incubated for 1 h at 37°C, washed with PBS, and sealed onto glass slides with 0.05 ml PBS containing 10% glycerol (Wako, Osaka, Japan) and 20 μg/ml DAPI (4'6-diamidino-2-phenylindole; Invitrogen). The cells were examined using a Keyence fluorescence microscope (Keyence, Osaka, Japan), and the green intensity of the phosphor-H2AX signal on digitized images was automatically analyzed using the software package Dynamic Cell Count (Keyence). Using this software package, the numbers and sizes of foci exhibiting high-intensity staining with gamma-H2AX (green) in each type of A172 cell population were determined in more than 100 areas per condition.

Statistical analysis

Values are presented as means ± standard errors. Statistical analyses were performed using the unpaired, two-tailed Student's *t*-test. A significance level of $P < 0.05$ was used for all analyses. The data on cell survival were fitted to the linear-quadratic dose relationship.

RESULTS

Detection of stemness in GSLCs

Figure 1 shows the characteristics of the GSLCs. To induce GSLCs, we cultured the A172 cells in SFM, as described above. Seven days after culturing in SFM, these cells were form-floating, neurosphere-like spheroid cells (Fig. 1A). In the Western blotting analysis, we found that two neural stem cell markers, Sox2 and Musashi, were more highly expressed in the GSLCs than in the A172 cells cultured in serum-containing medium as control cells (CCs) (Fig. 1B). However, no apparent CD133 expression was detected in either GSLCs or CCs that were cultured for 7 d. Therefore, we changed the CD133-detection assay for FACS analysis by using several time-points. In the FACS analysis, the ratio of CD133-positive GSLCs increased by 9% after 14 d, whereas the ratio of CD133-positive CCs was unchanged (Fig. 1C). The FACS analysis confirmed marked positivity in the WERI-Rb-1 (WE) cells, a retinoblastoma cell line used as a control (data not shown).

Radiosensitivity of GSLCs and CCs

The radiosensitivity of GSLCs was compared with that of CCs under gamma-ray or neutron-beam irradiation. Figure 2 shows the surviving fractions of A172 under the two culture conditions after gamma-ray or neutron-beam irradiation. After gamma-ray irradiation, GSLCs showed significantly greater radioresistance than CCs. On the other hand, after neutron-beam irradiation, there was no significant difference in the sensitivity between GSLCs and CCs. The D_{10} values were calculated by linear regression analysis from the survival curves shown in Fig. 2, and the D_{10} dose parameters for survival following irradiation and their RBEs are listed in Table 1. The D_{10} value represents the radiation dose that produces a survival fraction of 10%. To examine the difference in radiosensitivity between GSLCs and CCs, we referred to the resistance ratio. This ratio was calculated from the D_{10} dose of GSLCs per that of each respective CC by these two forms of irradiation. For example, under gamma-ray irradiation, the ratio of the D_{10} dose of GSLCs to that of CCs was 3.98/3.02 = 1.318. On the other hand, under neutron-beam irradiation, the D_{10} dose of GSLCs per that of CCs was 1.17/1.25 = 0.936. The resistance ratio of neutron beams was smaller than that of gamma rays. Consequently, neutron-beam irradiation overcame the resistance to gamma-ray irradiation in A172 GSLCs. In other words, these results suggested that A172 GSLCs, which were radioresistant to gamma rays, became sensitive to neutron beams.

Persistence of gamma-H2AX foci following irradiation

Figure 3 shows representative images of each type of A172 cells at 24 h after each type of irradiation. The fluorescence intensity of gamma-H2AX foci produced by neutron beams was stronger than that produced by gamma rays in both GSLCs and CCs, under the same staining conditions and the same photographic exposure time (Fig. 3). At a glance, the foci in both CCs and GSLCs produced by neutrons seemed larger than those produced by gamma rays. Figure 4A and B show the change in the numbers of gamma-H2AX foci following 4 Gy of gamma-ray or neutron irradiation in GSLCs and CCs induced from A172 cells. There were significantly more gamma-H2AX foci per cell in CCs than in GSLCs 24 h after gamma-ray irradiation. However, after neutron-beam irradiation, there was no apparent difference between GSLCs and CCs in the number of gamma-H2AX foci. Figure 4C and D show the distribution histograms of the size of foci induced in GSLCs and CCs, respectively, and Fig. 4E shows the mean size of gamma-H2AX foci at 24 h post-irradiation,

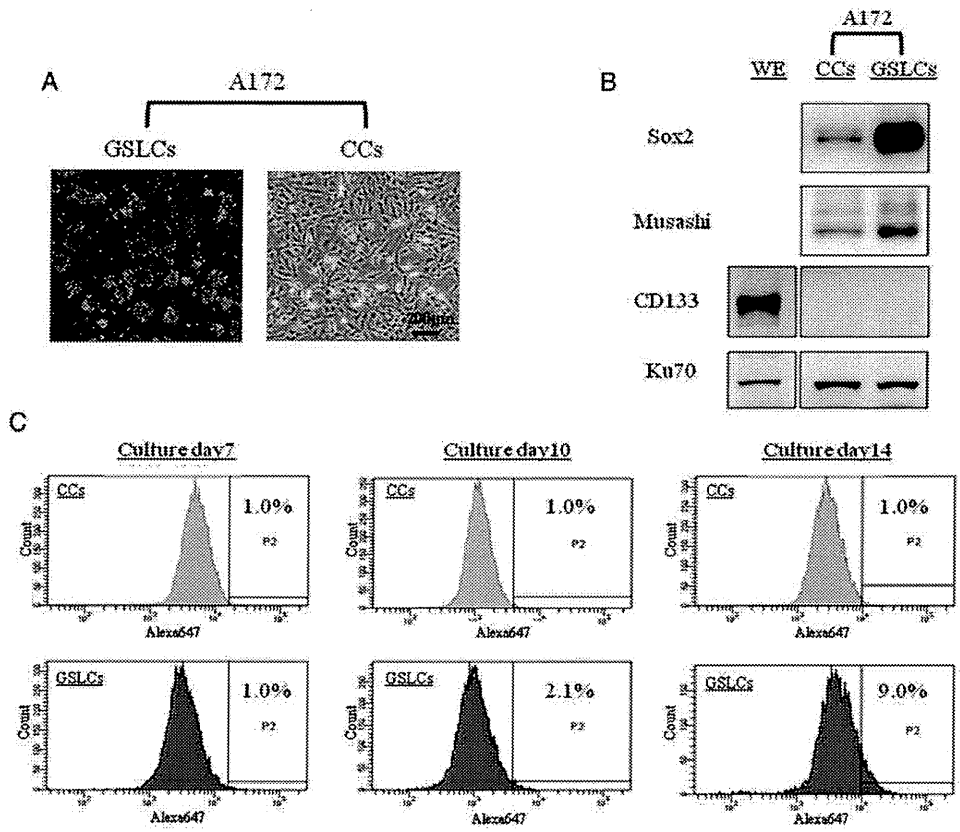

Fig. 1. Characteristics of the glioma stem-like cells. (**A**) The morphology of human glioma cell line A172 cultured for 7 d in serum-containing medium or serum-free medium. (**B**) The expression of typical stem cell marker proteins as examined by Western blot assays on Day 7 after culture. (**C**) The ratio of CD133-positive cells in FACS analysis; the number of days of culture is shown in each column, and the rate of CD-133-positive GSLCs was measured with a cutoff value obtained from the fluorescence intensity that occupied 1% by putative CD133-positive CCs in the total population. GSLCs = glioma stem-like cells; CCs: control cells; WE = WERI-Rb-1 (the retinoblastoma cell line used as a positive control for anti-CD133 Ab).

measured using the BZII image analysis system (Keyence). Figure 4C, D and E reveal definitively that neutron-beam irradiation induced larger gamma-H2AX foci than those observed after gamma-ray irradiation, not only in CCs but also in GSLCs of A172 cells. These results might suggest that DSBs were repaired more efficiently in GSLCs than in CCs following gamma-ray irradiation. In contrast, under neutron irradiation, the DNA DSBs were not repaired efficiently in either GSLCs or CCs.

DISCUSSION

Research on GSCs has been conducted for many years, and GSCs have been found to contribute to the recurrence and resistance to therapy of malignant gliomas [2–6]. The difficulty of treating GBM may be attributed to the existence of GSCs in GBM, judging from the numerous published findings about GSCs.

In previous reports, GSCs were isolated from glioma tissues as spheres cultured in SFM containing stem-cell mitogens, epidermal growth factor and fibroblast growth factor, which is the same method used to isolate neural stem cells from brain tissue [2–4, 17]. Because of the lack of serum and the low plating density, most of the cells die, except those that divide in response to the stem-cell mitogens. The growth-factor-responsive cells proliferate to form floating clusters called neurospheres [18]. In this study, we induced GSLCs from cells of the human GBM line A172 using the same isolation-GSCs method as described previously [12]. In SFM containing the stem-cell mitogens, GSLCs were produced as neurosphere-like spheroid cells, and expressed neural stem cell markers such as Sox2 and Musashi (Fig. 1A and B) on Day 7 after induction. Actually, CD133 was hardly detected in Western blot analysis after 7 d of culture. Therefore, we performed FACS analyses and determined the ratio of CD133 positivity between GSLCs and CCs by kinetics study. The CD133-positive fraction in GSLCs

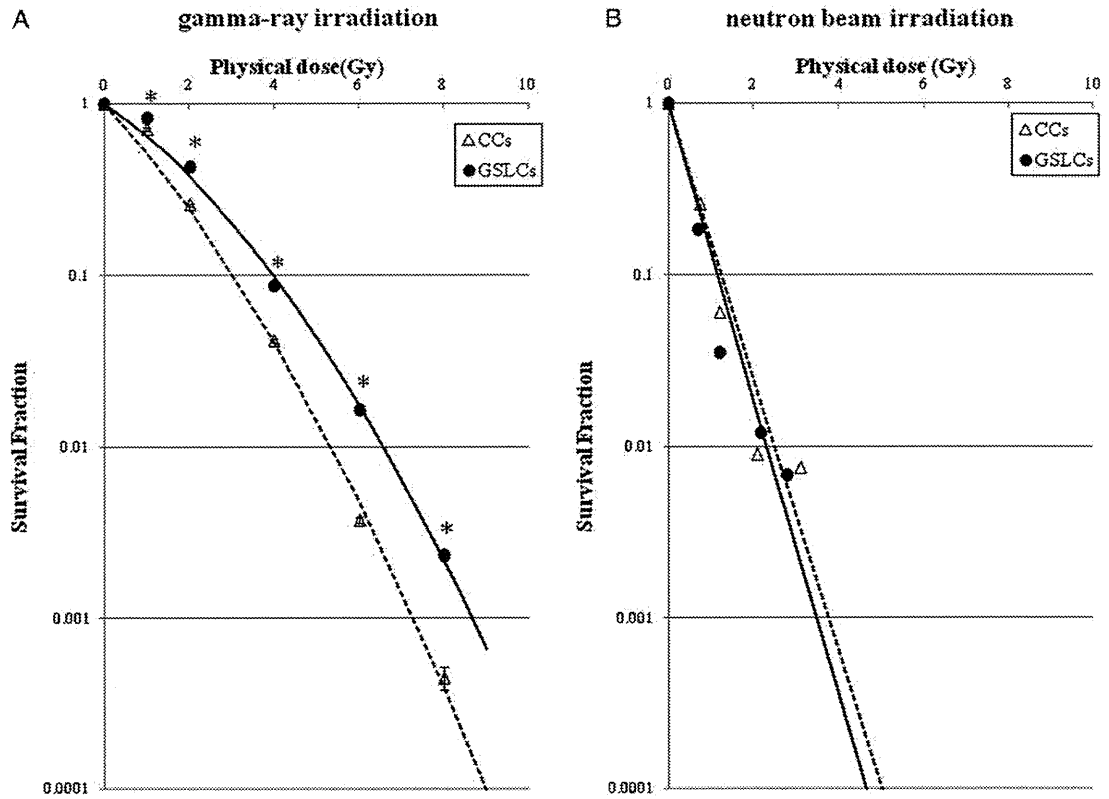

Fig. 2. Cell survival curves of GSLCs induced from A172 cells cultured with serum-free medium and CCs cultured with normal medium after gamma-ray (**A**), or neutron-beam irradiation (**B**). The data are fitted with a linear quadratic model. Bars represent the standard errors based on three independent experiments. $^*P < 0.05$ compared with the survival fraction of GSLCs and CCs. GSLCs = glioma stem-like cells; CCs = control cells.

Table 1. D_{10} physical dose and RBE (relative biological effectiveness)

	Irradiation	
(CCs)	**gamma rays**	**neutron beams**
D_{10} physical dose	3.02	1.25
RBE[a]		2.42
(GSLCs)		
D_{10} physical dose	3.98	1.17
RBE		3.40
Resistance ratio[b](GSLCs/CCs)	1.318	0.936

[a]The ratio of the D_{10} physical dose compared to that of gamma rays. [b]The ratio of the dose of radiation necessary to obtain the D_{10} endpoint from GSLCs to that necessary in CCs. GSLCs = glioma stem-like cells, CCs = control cells, D_{10} = the radiation dose that produces a surviving fraction of 10%.

increased gradually in comparison with that in CCs day by day, and on Day 14, 9% of GSLCs were CD133-positive, although many GSLCs were still negative for CD133. In addition, 30 d of induction culture resulted in a higher percentage of CD133-positive GSLCs—up to 21% (data not shown). We speculate that it took a long time for CD133-positive cells to be refined in the SFM, and thus there was an insufficient number of CD133-positive cells for detection by Western blot analysis on Day 7. Indeed, CD133 positivity in our GSLCs from A172 on Day 7 was still small in number, but other stemness markers increased compared with CCs, and CD133 is not always a good GSC marker [19–21]. In addition, GSLCs induced by this method showed the upregulation of ATP-binding cassette transporter G2 and increased chemo-resistance in comparison with CCs (data not shown and manuscript in preparation). Above all, these GSLCs from A172 were somewhat radioresistant for low-LET gamma rays. Thus, we judged that these GSLCs were adequate for our further experiments. In any event, GSLCs had some degree of stemness. Actually, we tried to induce GSLCs from three GBM lines. Among them, GSLC from A172 was most prominent with GSC phenotype and apparent radioresistance to low-LET γ-rays. Thereafter, we used GSLCs from A172 in the current studies. We assessed the radiosensitivity of GSLCs using colony-forming assay on

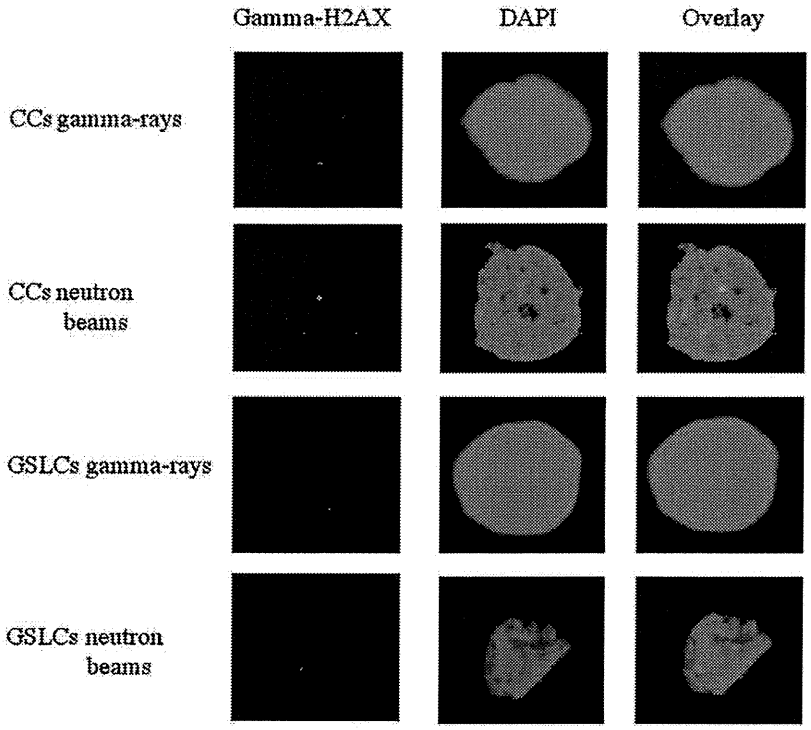

Fig. 3. Representative images of nuclear gamma-H2AX foci of CCs and GSLCs in A172. These cells were irradiated with different types of beams (total physical dose = 4 Gy) and fixed at 24 h post-irradiation for gamma-H2AX detection. DAPI = staining of nuclear DNA; Gamma-H2AX = staining of gamma-H2AX foci; GSLCs = glioma stem-like cells; CCs = control cells.

Day 7. Although, there might be a possibility of change in radiosensitivity associated with change of expression of CD133, especially in the later period of the induction of GSLCs, such as on Day 28, in the previous report [22], A172 CCs did not express CD 133, while radiation-induced GSLCs of A172 cells did express CD133. This is in accord with our experiment.

To evaluate the difference in radiosensitivity between GSLCs and CCs, we irradiated these cells with gamma rays or neutron beams, and found that the latter could overcome the radioresistance of GSLCs to gamma rays (Fig. 2 and Table 1). To obtain neutron beams, we used the Heavy Water Column of the KUR. These neutron beams consisted of fast, epithermal and thermal neutrons. Each neutron beam produced proton particles by elastic scattering ($^{1}H(n,n)^{1}H$) or nitrogen capture reaction ($^{14}N(n,p)^{14}C$) at irradiation, and these particles exhibited high-LET radiation. The LET of proton particles produced by the former reaction was about 50 keV/μm, and that produced by the latter reaction was about 35 keV/μm, whereas the gamma rays exhibited low-LET radiation. Therefore, it can be concluded that high-LET radiation can better overcome the radioresistance of GSLCs in comparison with low-LET irradiation. Ionizing radiation produces a broad spectrum of molecular lesions in DNA, including single-strand breaks, DSBs, and a great variety of base damages. DSBs are the most toxic form of DNA damage, because a single unrepaired DSB can lead to abnormal mitosis with losses of large fragments of DNA [23]. Further, it is generally accepted that high-LET radiation induces more serious DNA DSBs than low-LET radiation [11, 24]. In the current study, we demonstrated that high-LET radiation could damage GSLCs that were resistant to low-LET gamma rays. As previously described, GSCs have a large capacity to repair DSBs induced by low-LET radiation [5]. However, it was uncertain whether or not high-LET radiation could cause serious DSBs that were unrepairable, even in GSCs.

To clarify the response to DNA DSBs induced by gamma rays or neutron beams, we employed a gamma-H2AX assay. From a previous report, we judged the persistence of gamma-H2AX foci 24 h after treatment as unrepairable DSB [25]. GSLCs had a larger restoration capacity for DSBs than CCs after low-LET radiation, but could not repair DSBs sufficiently after high-LET radiation (Fig. 4A and B). Because reduced survival was accompanied by the persistence of DNA damage, as evidenced by the persistence of gamma-H2AX foci after irradiation [26], high-LET radiation could produce persistence of DSBs and induce fatal damage even

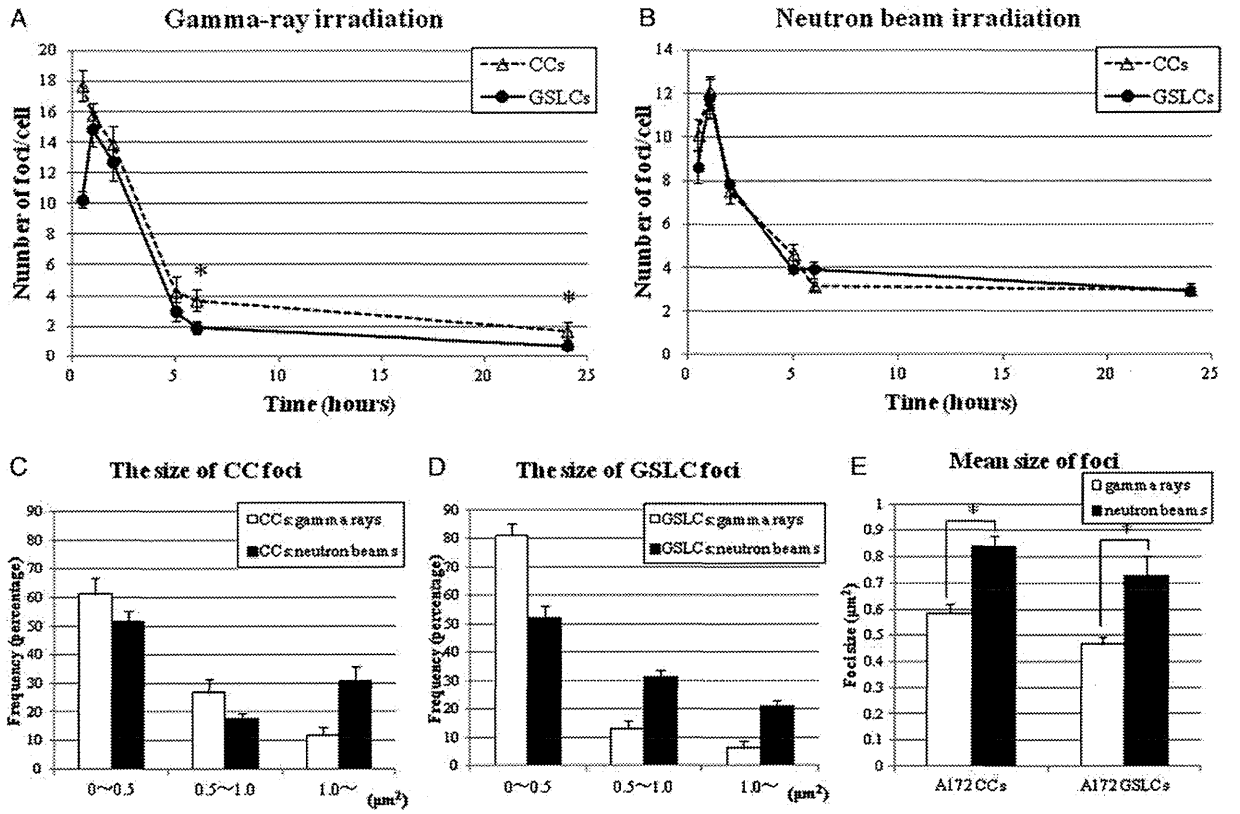

Fig. 4. Change in the number of induced nuclear gamma-H2AX foci and the histograms of gamma-H2AX foci size, at the times indicated post-irradiation in A172. These cells were irradiated with different types of beams (total physical dose = 4 Gy). (**A**) and (**B**) The numbers of gamma-H2AX foci per cell of GSLCs and CCs in A172 after the different types of radiation. (**C**) and (**D**) Distribution of gamma-H2AX foci sizes for A172 at 24 h post-irradiation. (**E**) Mean gamma-H2AX foci size for each type of A172 cells at 24 h post-irradiation. Bars represent the standard errors. $^*P < 0.05$ compared with gamma-H2AX foci per cell in GSLCs and CCs. GSLCs = glioma stem-like cells; CCs = control cells.

in GSLCs. In fact, it has been reported that to evaluate gamma-H2AX foci in cells exposed to high-LET radiation, the size of the foci should be considered, since high-LET radiation can cause larger gamma-H2AX foci than low-LET radiation [11, 27]. We therefore investigated not only the numbers of foci but also their size after 24 h irradiation by both types of radiation, and found that high-LET radiation could cause larger gamma-H2AX foci than low-LET radiation in both GSLCs and CCs (Figs. 3, 4C, 4D and 4E). As Fig. 4E shows, high-LET radiation led to significantly larger gamma-H2AX foci than low-LET radiation did, in both GSLCs and CCs. Therefore, it is thought that high-LET radiation could cause more serious DNA DSBs than low-LET radiation, even in GSLCs. In the previous report [28], low-LET irradiation might produce relatively large foci with time. In our experiment we demonstrated that high-LET particles produce larger foci in GSLC than low-LET gamma rays.

Indeed, under both gamma-ray and neutron-beam irradiation, more than half of all gamma-H2AX foci were small (0–0.5 μm^2). It is speculated that the neutron beams from KUR formed a wide-range beam that included gamma rays and secondary gamma rays. At the absorbed dose of 4 Gy, the compositions of fast, epithermal and thermal neutrons as well as of gamma rays were 25.5%, 2.5%, 22% and 50%, respectively. Almost half of the neutron beam components of the absorbed dose were induced by gamma rays, which could explain why small foci were induced mainly by gamma rays, even under neutron-beam irradiation. As described above, Fig. 3 also shows that the fluorescence intensity of gamma-H2AX foci after neutron irradiation was higher than that after gamma-ray irradiation. This may explain why high-LET radiation causes more intense DNA damage than low-LET radiation. A previous study showed that high-LET radiation, such as that from heavy ion therapy, had several potential advantages over low-LET radiation due to its induction of complex DNA damage that was not easily repaired [29], and may have an advantage over low-LET radiation for cancer stem-like cells [30]. Thus, our data also support the potential for use of high-LET radiation for GSCs.

Heavy ion treatment and BNCT are recognized as forms of high-LET radiation. In a previous report, when chemo-irradiation was combined with carbon ion therapy, the median survival time of GBM patients was 17 months [31]. In another report, BNCT followed by X-ray radiation therapy led to a median survival time of GBM patients of 21.3 months, even without chemotherapy [9]. Although both of these reports involved small numbers of patients, the results suggested that, since these high-LET radiations were effective even for GSCs in a clinical setting, patients could show prolonged survival. At the moment these treatment modalities are still at the clinical trial stage, but they may improve the standard treatment for GBM.

Although various treatments for GBM have been tried, an unfavorable prognosis can be expected with the current standard treatment. In the present study, we demonstrated that high-LET radiation may be able to overcome GSC resistance to low-LET radiation. It is necessary to further investigate the usefulness of high-LET radiation for the control of GSCs. High-LET radiation therapies such as BNCT or heavy ion therapy have very important roles in further treatment for therapy-resistant GBM.

CONFLICT OF INTEREST

The authors have no conflicts of interest to disclose.

FUNDING

This work was supported by a Grant-in-Aid for Scientific Research (B) (23390355) from the Japanese Ministry of Education, Culture, Sports, Science and Technology to S-IM.

REFERENCES

1. Stupp R, Mason WP, van den Bent MJ *et al.* Radiotherapy plus concomitant and adjuvant temozolomide for glioblastoma. *N Engl J Med* 2005;**352**:987–96.
2. Singh SK, Clarke ID, Terasaki M *et al.* Identification of a cancer stem cell in human brain tumors. *Cancer Res* 2003;**63**: 5821–8.
3. Singh SK, Hawkins C, Clarke ID *et al.* Identification of human brain tumour initiating cells. *Nature* 2004;**432**:396–401.
4. Yuan X, Curtin J, Xiong Y *et al.* Isolation of cancer stem cells from adult glioblastoma multiforme. *Oncogene* 2004;**23**: 9392–400.
5. Bao S, Wu Q, McLendon RE *et al.* Glioma stem cells promote radioresistance by preferential activation of the DNA damage response. *Nature* 2006;**444**:756–60.
6. Chang CJ, Hsu CC, Yung MC *et al.* Enhanced radiosensitivity and radiation-induced apoptosis in glioma CD133-positive cells by knockdown of SirT1 expression. *Biochem Biophys Res Commun* 2009;**380**:236–42.
7. Miyatake S, Kawabata S, Kajimoto Y *et al.* Modified boron neutron capture therapy for malignant gliomas performed using epithermal neutron and two boron compounds with different accumulation mechanisms: an efficacy study based on findings on neuroimages. *J Neurosurg* 2005;**103**:1000–9.
8. Miyatake S, Tamura Y, Kawabata S *et al.* Boron neutron capture therapy for malignant tumors related to meningiomas. *Neurosurgery* 2007;**61**:82–90; discussion 90–1.
9. Kawabata S, Miyatake S, Kuroiwa T *et al.* Boron neutron capture therapy for newly diagnosed glioblastoma. *J Radiat Res* 2009;**50**:51–60.
10. Miyatake S, Kawabata S, Yokoyama K *et al.* Survival benefit of Boron neutron capture therapy for recurrent malignant gliomas. *J Neurooncol* 2009;**91**:199–206.
11. Kinashi Y, Takahashi S, Kashino G *et al.* DNA double-strand break induction in Ku80-deficient CHO cells following boron neutron capture reaction. *Radiat Oncol* 2011;**6**:106.
12. Qiang L, Yang Y, Ma YJ *et al.* Isolation and characterization of cancer stem like cells in human glioblastoma cell lines. *Cancer Lett* 2009;**279**:13–21.
13. Sakurai Y, Kobayashi T. Characteristics of the KUR Heavy Water Neutron Irradiation Facility as a neutron field with variable energy spectra. *Nucl Instrum Meth A* 2000;**453**:569–96.
14. Kobayashi T, Kanda K. Analytical calculation of boron-10 dosage in cell nucleus for neutron capture therapy. *Radiat Res* 1982;**91**:77–94.
15. Kitao K. A method for calculating the absorbed dose near interface from 10B(n, alpha)7Li reaction. *Radiat Res* 1975; **61**:304–15.
16. Ohnishi T, Mori E, Takahashi A. DNA double-strand breaks: their production, recognition, and repair in eukaryotes. *Mutat Res* 2009;**669**:8–12.
17. Fukaya R, Ohta S, Yamaguchi M *et al.* Isolation of cancer stem-like cells from a side population of a human glioblastoma cell line, SK-MG-1. *Cancer Lett* 2010;**291**:150–7.
18. Vescovi AL, Galli R, Reynolds BA. Brain tumour stem cells. *Nat Rev Cancer* 2006;**6**:425–36.
19. Baumann M, Krause M, Hill R. Exploring the role of cancer stem cells in radioresistance. *Nat Rev Cancer* 2008;**8**:545–54.
20. Baumann M, Krause M, Thames H *et al.* Cancer stem cells and radiotherapy. *Int J Radiat Biol* 2009;**85**:391–402.
21. Ogden AT, Waziri AE, Lochhead RA *et al.* Identification of A2B5+CD133– tumor-initiating cells in adult human gliomas. *Neurosurgery* 2008;**62**:505–14; pdiscussion 514–5.
22. Shimura T, Noma N, Oikawa T *et al.* Activation of the AKT/cyclin D1/Cdk4 survival signaling pathway in radioresistant cancer stem cells. *Oncogenesis* 2012;**1**:e12.
23. van Gent DC, Hoeijmakers JH, Kanaar R. Chromosomal stability and the DNA double-stranded break connection. *Nat Rev Genet* 2001;**2**:196–206.
24. Leatherbarrow EL, Harper JV, Cucinotta FA *et al.* Induction and quantification of gamma-H2AX foci following low and high LET-irradiation. *Int J Radiat Biol* 2006;**82**:111–8.
25. Schmid TE, Dollinger G, Beisker W *et al.* Differences in the kinetics of gamma-H2AX fluorescence decay after exposure to low and high LET radiation. *Int J Radiat Biol* 2010;**86**: 682–91.
26. Prevo R, Deutsch E, Sampson O *et al.* Class I PI3 kinase inhibition by the pyridinylfuranopyrimidine inhibitor PI-103 enhances tumor radiosensitivity. *Cancer Res* 2008;**68**:5915–23.
27. Ibanez IL, Bracalente C, Molinari BL *et al.* Induction and rejoining of DNA double strand breaks assessed by H2AX

phosphorylation in melanoma cells irradiated with proton and lithium beams. *Int J Radiat Oncol Biol Phys* 2009;**74**: 1226–35.

28. Yamauchi M, Oka Y, Yamamoto M *et al.* Growth of persistent foci of DNA damage checkpoint factors is essential for amplification of G1 checkpoint signaling. *DNA Repair (Amst)* 2008; **7**:405–17.
29. Okayasu R, Okada M, Okabe A *et al.* Repair of DNA damage induced by accelerated heavy ions in mammalian cells proficient and deficient in the non-homologous end-joining pathway. *Radiat Res* 2006;**165**:59–67.
30. Cui X, Oonishi K, Tsujii H *et al.* Effects of carbon ion beam on putative colon cancer stem cells and its comparison with X-rays. *Cancer Res* 2011;**71**:3676–87.
31. Mizoe JE, Tsujii H, Hasegawa A *et al.* Phase I/II clinical trial of carbon ion radiotherapy for malignant gliomas: combined X-ray radiotherapy, chemotherapy, and carbon ion radiotherapy. *Int J Radiat Oncol Biol Phys* 2007;**69**:390–6.

定位的放射線治療
18：43～49，2014

悪性神経膠腫の放射線治療後再発例に対するホウ素中性子捕捉療法の成績

Clinical results of boron neutron capture therapy on previously irrediated patients with recurrent malignant glioma

川端　信司[1]、平松　亮[1]、古瀬　元雅[1]、松下　葉子[1]、二村　元[1]、
大西　宏之[1]、黒岩　敏彦[1]、近藤　夏子[2]、鈴木　実[2]、
櫻井　良憲[3]、田中　浩基[3]、小野　公二[2]、宮武　伸一[1]

[1]大阪医科大学医学部　脳神経外科
[2]京都大学　原子炉実験所

要旨：ホウ素中性子捕捉療法（BNCT）は、ホウ素（^{10}B）が中性子を捕獲し、細胞レベルで生じた核反応から得られる粒子線を利用した腫瘍選択的治療法である。

放射線治療歴を有した34例の再発悪性神経膠腫を対象に検討を行った。再発悪性神経膠腫に対する標準的治療法は確立されておらず、解析は予後因子別解析を利用して行った。

全生存期間中央値は11.2（8.9-12.4）ヶ月であり、予後不良とされるサブグループでは11.0ヶ月と良好であった（vs 4.4）。予後因子は、BNCT時の組織診断、ステロイド・テモゾロミド治療歴、腫瘍局在（左右）となり、腫瘍サイズはリスクとはならなかった。

BNCTは原子炉を利用するという障壁により、広く受け入れられるに至らなかった。近年、加速器を中性子源としたBNCT治療装置が開発され、第一相試験が進行中である。本報告では、同様な対象症例に対する原子炉BNCTの良好な治療成績が示された。

key words：神経膠腫、再発、ホウ素中性子捕捉療法、放射線治療、再照射

はじめに

放射線治療後の再発悪性神経膠腫に対しても積極的に放射線治療が行われ成績を上げているが、これまでの報告ではその効果は限定的であり、より効果的かつ安全な照射法が望まれる。ホウ素中性子捕捉療法（BNCT）は、ホウ素（^{10}B）が中性子を効率よく捕獲し、生じた核反応から得られる粒子線が細胞一個に相当する飛程で全エネルギーを放出することを利用した高LET（Linear Energy Transfer、線エネルギー付与）の腫瘍選択的治療法である（figure 1）[1)]。

I. 対象と方法

原子炉中性子源を用いたBNCTで治療を実施した再発悪性神経膠腫に対し、後方視的に解析を加えた。本解析の対象となった患者は、当施設で治療を行った再発悪性神経膠腫症例34例で、男性22例、女性12例である。BNCT治療時の平均年齢は50.5（15～74）歳で、全例

別冊請求先：〒569-8686　大阪府高槻市大学町2-7
大阪医科大学　脳神経外科
川端　信司　　TEL：072-683-1221　FAX：072-683-4064
E-mail：neu046@poh.osaka-med.ac.jp

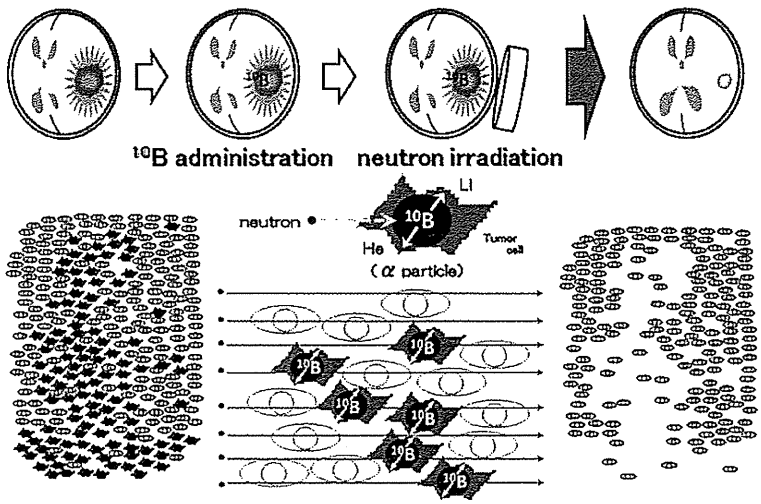

Figure 1 The principle of boron neutron capture therapy (BNCT).

BNCT is a binary approach: A boron-10 (^{10}B)-labeled compound is administered that delivers high concentrations of ^{10}B to the target tumor relative to surrounding normal tissues. This is followed by irradiation with thermal neutrons or epithermal neutrons that become thermalized at depth in tissues. About one cell size level short range high energy of the alpha and ^{7}Li particles released from the ^{10}B (n, alpha) ^{7}Li neutron capture reaction make tumor selective killing without damage for adjacent normal brain tissue.

が初発時もしくは再発／悪性転化時にX線分割外照射を中心とした放射線治療を受けている。照射時のKPS (Karnofsky Performance Status) の中央値は80 (50～100) で、画像上の再発腫瘍体積は平均32mLであった。

BNCTは、熱外中性子による非開頭照射で行い、照射前に実施したBNCT用の治療薬であるホウ素化合物 (BPA; borono-phenylalanine) をトレーサーとしたPET (^{18}F-BPA PET) 検査によるホウ素化合物の集積比および治療当日の血中ホウ素濃度から個々の患者の線量計画を行った (Figure 2) [2]。中性子源としては、主として京都大学原子炉実験所 (大阪府・熊取) KURRIを利用し、メンテナンス等の事由で使用不可の期間に関しては日本原子力開発研究機構 (茨城県・東海) JRR-4を利用して行った。

また予後因子の解析に際しては、2007年にNABTT (New Approaches to Brain Tumor Therapy CNS Consortium) からJournal of Clinical Oncologyに報告された再発悪性膠腫に対するRPA (recursive partitioning analysis) 分類で用いられた予後因子 (Table 1) [3]を中心に、BNCTにおいて考慮すべき項目を含め検討した。すべての統計解析はJMP Pro 9 (SAS Institute Japan) を使用し行った。

II. 結果

対象患者全体でのBNCT後の生存期間中央値 (MST; median survival time) は、11.2 (95%CI: 8.9 – 12.4) ヶ月であった。今回の解析対象とした項目は、年齢、性別、BNCT時のKPS、初発時の組織型、再発時の組織型、腫瘍局在、ステロイド使用歴、テモゾロミド治療歴、腫瘍体積である。

単一の項目で予後と有意に相関した因子は、BNCT時の組織型 (膠芽腫 (glioblastoma、GB) 10.3ヶ月、非GB 15.0ヶ月、$p = 0.045$)、ステロイド使用 (使用例 9.6ヶ月、非使用例 12.8ヶ月)、テモゾロミド治療歴 (あり 10.3ヶ月、なし

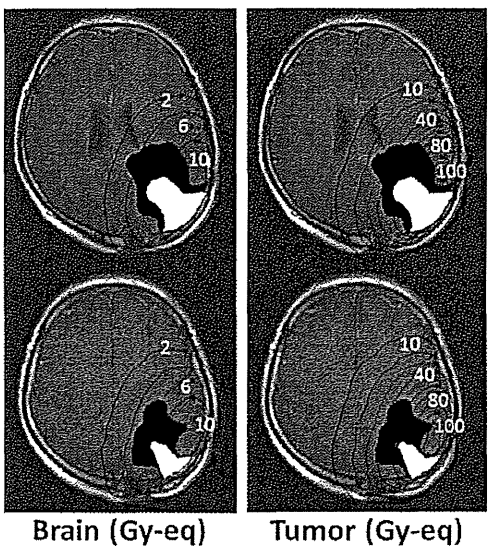

Figure 2 Dose planning of boron neutron capture therapy (BNCT).

Dose planning of neutron capture therapy for the tumor (right) and for the normal brain (left). (Gy-Eq: gray equivalent, star: air instillation to the tumor removed cavity)
In this case, tumor volume was 70mL (black area; tumor; white area; cavity with fluid) and >40Gy was irradiated for 75% and >30Gy for 87% of gross tumor volume. Peak dose for normal brain and skin was 11 and 7 Gy-eq, respectively.

12.4ヶ月)、腫瘍局在 (左半球 8.6ヶ月、右半球 11.7ヶ月) であった。年齢、BNCT時のKPSに関しては、予後に対してカットオフは得られず、また対照としたNABTT-RPAで示された病変の前頭葉限局 (Risk Ratio 1.88, 95% CI: 1.36 - 2.60 p=.0001) [3]に関してもBNCT治療例においては有意な相関は得られなかった (前頭葉限局 10.3ヶ月、それ以外 11.3ヶ月、p=0.131)。腫瘍体積に関しては、カットオフとなった8mL未満の例 (n=7) でMST = 12.8ヶ月、8mL以上の例で11.0ヶ月となり両者に有意差は無かった。中央値である32mL以上の患者 (平均腫瘍体積は52mL) のMSTは 11.4ヶ月であった。また再発時の組織型をGBに限ると、平均腫瘍体積は36mLであり、MSTは10.4ヶ月であった (Table 2)。

最終的なNABTT-RPAクラス別の解析では、最も予後不良とされたclass 3 + 7でのMST = 4.4 (3.6 – 5.4ヶ月) ヶ月 (Table 1) [3]に対し、BNCT治療群は11.0ヶ月 (7.8 – 11.6ヶ月) となった。

III. 考察

再発悪性神経膠腫の予後は極めて不良であり、特に既放射線治療例での治療には難渋する。手術や放射線の追加・再照射も行われてきたが、再発からの生存期間は6ヶ月程度とされる。我々はこれまでにも、初発・再発の悪性神経膠腫や悪性髄膜腫に対する効果を示してきたが[4,5,6]、既放射線治療の再発例におけるBNCTの治療効果も良好で、当施設ではこれまで他の治療法では得られ難い画像上の縮小効果も報告してきた[7-9]。

脳実質内に浸潤性に発育する悪性脳腫瘍、特に悪性神経膠腫は、浸潤領域の脳細胞が機能していると考えられ、腫瘍を細胞レベルで標的とする選択的治療が理想となる。ホウ素中性子捕捉療法 (boron neutron capture therapy; BNCT) は、生物学的に腫瘍細胞を標的とする粒子線治療であり、浸潤性発育を特徴とする外科的治癒切除が不能な腫瘍に対する治療効果が期待される[10]。BNCTの骨子は、腫瘍細胞にホウ素－10 (boron-10、^{10}B) 化合物を取り込ませた後に患部に中性子を照射することにより、高LETのα粒子が腫瘍細胞ひとつ分に相当する飛程 (約10μm) で放出されることによってホウ素が集積した腫瘍細胞のみを選択的に破壊するという、細胞生物学的な標的手法にある。特筆すべきは、投与するホウ素化合物および照射する中性子が、各々単一では細胞障害性が極めて低いことで、両者が相まって始めて殺細胞効果を示すbinary approachであることである[1]。

BNCTは細胞レベルで選択性を有することから、正常組織内に浸潤性に発育する腫瘍や周囲正常臓器に混在した癌に対する治療効果が期待され、これまでにも多数の臨床試験・研究が行われてきた[11]。あらゆる治療に抵抗性を示し、有効な治療手段の限られる神経膠

腫、特に神経膠芽腫（WHOグレード4）においては期待が高く、これまでにBNCTで治療がなされた症例の多くは初発の悪性神経膠腫であった。

Table 1 Prognostic factors for survival in adult patients with recurrent glioma enrolled onto the NABTTclinical trials

class	results of the recursive partitioning analysis (RPA).	survival time (median)	
1	Initial histology = Not GB, KPS = 80-100, location (Frontal only)	25.7	months
2	Initial histology = Not GB, KPS = 80-100, location (Other)	17.2	months
3	Initial histology = Not GB, KPS = 60-70	3.8	months
4	Initial histology = GB, Age < 50, KPS = 90-100	10.4	months
5	Initial histology = GB, Age < 50, KPS = 60-80	5.6	months
6	Initial histology = GB, Age >= 50, Steroids (No)	6.4	months
7	Initial histology = GB, Age >= 50, Steroids (Yes)	4.9	months

GB, glioblastoma; KPS, Karnofsky performance score.
*Carson et al, J Clin Oncol 25: 2601-6, 2007 [2]

Table 2 Overview of re-irradiation for recurrent malignant gliomas with large targeted volumes

	no of cases	Irradiation	tumor volume (median, mL)	overall survival (median)	
Cho et al., 1999 (12)	27 GB / 19 grade III	SRS	10	11	months
	15 GB / 10 grade III	fractionated SRT	25	12	months
Lederman et al., 2000 (13)	88 GB	hypofractionated SRT	33	7.0	months
(	38 GB		<30	9.4	months)
(	50 GB		>30	5.7	months)
					months
Voynov et al., 2002 (14)	5 GB / 5 grade III	IMRT	35	10.1	months
Hall et al., 1995 (15)	26 GB / 9 grade III	SRS	28	8.0	months
Combs et al., 2005 (16)	53 GB	fractionated SRT	48	8	months
Patel et al., 2009 (17)	10 GB	fractionated SRT	51	7.5	months
Kawabata et al, present series	26 GB	BNCT	36	10.3	months

abbreviations: GB, glioblastoma; SRS, stereotactic radiosurgery; SRT, stereotactic radiotherapy; IMRT, intensity-modulated radiotherapy; BNCT, boron neutron capture therapy

当施設が利用する京都大学原子炉実験所(KURRI)では、1990年から悪性神経膠腫に対する治療が行われたが、多くの再発例を含みながらも3年生存率で20%以上と従来の治療に比べ約2倍に向上した[12]。しかし当時利用されていた熱中性子では深部での十分な線量が得られず、さらなる改善が必要であると考えられていた。その後中性子およびホウ素化合物が改良され、脳腫瘍以外の癌に対しても良好な成績が示されるに至った[11]。

今回我々が示した再発悪性神経膠腫に対する治療成績は、BNCTからのMSTが約11ヶ月と良好であるが、再発神経膠腫には比較対象となる標準治療群が存在せず、この数値のみをもって有効とするには無理がある。そこでこのBNCTによる治療成績を、再発悪性神経膠腫の臨床試験(NABTTの10個のphase I, IIに登録された333例の解析[3])から得られた予後因子による分類と比較した。これによると、最も予後不良とされたclass 3 + 7でのMST 4.4 (3.6 – 5.4) ヶ月[3]に対し、BNCT治療群は11.0 (7.8 – 11.6) ヶ月と大きく上回っていた。BNCTはこれまでに予後不良、すなわち治療に難渋する患者群に対しその効果が非常に高いことが示され、これは初発の膠芽腫症例に対するBNCTでも同様にみられた現象である[13]。

再発悪性神経膠腫に対する再照射治療として、定位的照射が良好な成績を示してきたが、照射法の特徴から標的腫瘍体積に制限がかかる(Table 2)[14-19]。再発後のMSTは定位的照射において10ヶ月以上の成績を示すものも多いが、試験対象とする適格基準にも見られるように、腫瘍体積が比較的小さいものに限られる。腫瘍体積の大きい例に対しても、安全性を確保しつつ腫瘍に対し高線量を付与可能な分割による定位的照射が行われている。しかしながら腫瘍体積が大きいものでは成績が劣る傾向があり、この点においてBNCTはより有利と考えられる。過去の報告例でみると、やはり一回照射のSRS (stereotactic radiosurgery) には限界が見える。比較的腫瘍体積の小さなものでは非常に有効な手段と考えるが[14]、多くの再発例でみられる大きな腫瘍になると、定位的照射法では腫瘍に付与可能な線量に制限があり、生存期間の延長効果はわずかとなる[17]。分割によってより安全な高線量照射が可能となっているが、GBに限った試験でのMSTは7～8ヶ月と劣り、やはり腫瘍体積に影響されている[15,18,19]。BNCTにおいても腫瘍体積8mLが最も良いカットオフと算出され、8mL以上の例でのMSTが12.8ヶ月、8mL未満の例では11.0ヶ月と小さい腫瘍の群で若干高い効果がみられたが、両者に有意差は無い。また中央値32mL以上(平均腫瘍体積は52mL)のMSTは11.4ヶ月であり、大きな腫瘍に対しても高い治療効果が示された。

BNCTは、悪性神経膠腫の放射線治療後再発例に対し、安全に施行しうる有効な治療手段であり、生命予後を改善した。腫瘍選択的照射であるBNCTでは、特に予後不良とされるサブグループ・治療困難例において有効性が高い傾向が見られた。

IV. 結語

我々の改良型BNCTによる再発悪性神経膠腫の治療では、特に予後不良とされるグループにおいて高い治療効果が示された。悪性神経膠腫のごとく浸潤性に発育する腫瘍では、周囲組織への影響が懸念されるが、BNCTは細胞選択的粒子線治療という特徴から、正常細胞への影響が少なく高線量による強力な放射線照射が可能となるためと考える。

文献

1) Barth RF, Coderre JA, Vicente MG, et al: Boron neutron capture therapy of cancer: current status and future prospects. Clin Cancer Res 11: 3987-4002, 2005.
2) Kawabata S, Miyatake S, Kajimoto Y, et al: The early successful treatment of glioblastoma patients with modified boron neutron capture therapy. Report of two cases. J Neurooncol 65: 159-65, 2003.
3) Carson KA, Grossman SA, Fisher JD, et al: Prognostic factors for survival in adult patients with recurrent glioma enrolled onto the new approaches to brain tumor

therapy CNS consortium phase I and II clinical trials. J Clin Oncol 25: 2601-6, 2007.

4) 川端信司, 宮武伸一, 宮田至朗ら: ホウ素中性子捕捉療法による悪性神経膠腫の治療効果. 定位的放射線治療 13: 23-30, 2009.

5) 川端信司, 平松亮, 宮田至朗ら: ホウ素中性子捕捉療法によるる悪性髄膜腫の治療成績. 定位的放射線治療 17: 75-81, 2013.

6) Miyatake S, Kawabata S, Yokoyama K, et al: Survival benefit of Boron neutron capture therapy for recurrent malignant gliomas. J Neurooncol 91: 199-206, 2009.

7) Hiramatsu R, Kawabata S, Furuse M, et al: Identification of early and distinct glioblastoma response patterns treated by boron neutron capture therapy not predicted by standard radiographic assessment using functional diffusion map. Radiat Oncol 8: 192, 2013.

8) Kawabata S, Hiramatsu R, Kuroiwa T, et al: Boron neutron capture therapy for recurrent high-grade meningiomas. J Neurosurg 119: 837-44, 2013.

9) Miyatake S, Kawabata S, Kajimoto Y, et al: Modified boron neutron capture therapy for malignant gliomas performed using epithermal neutron and two boron compounds with different accumulation mechanisms: an efficacy study based on findings on neuroimages. J Neurosurg 103: 1000-9, 2005.

10) Kawabata S, Matsushita Y, Furuse M, et al. Clinical Study on Modified Boron Neutron Capture Therapy for Newly Diagnosed Glioblastoma. In Chen CC (ed). Advances in the Biology, Imaging and Therapies for Glioblastoma. Rijeka, Croatia: InTech, 325-38, 2011.

11) Barth RF, Vicente MG, Harling OK, et al: Current status of boron neutron capture therapy of high grade gliomas and recurrent head and neck cancer. Radiat Oncol 7: 146, 2012.

12) 小野公二, 増永慎一郎, 高垣政雄ら: BNCTによる悪性神経膠腫の治療成績. 臨床放射線 44: 227-33, 1999.

13) Kawabata S, Miyatake S, Hiramatsu R, et al: Phase II clinical study of boron neutron capture therapy combined with X-ray radiotherapy/temozolomide in patients with newly diagnosed glioblastoma multiforme--study design and current status report. Appl Radiat Isot 69: 1796-9, 2011.

14) Cho KH, Hall WA, Gerbi BJ, et al: Single dose versus fractionated stereotactic radiotherapy for recurrent high-grade gliomas. Int J Radiat Oncol Biol Phys 45: 1133-41, 1999.

15) Lederman G, Wronski M, Arbit E, et al: Treatment of recurrent glioblastoma multiforme using fractionated stereotactic radiosurgery and concurrent paclitaxel. Am J Clin Oncol 23: 155-9, 2000.

16) Voynov G, Kaufman S, Hong T, et al: Treatment of recurrent malignant gliomas with stereotactic intensity modulated radiation therapy. Am J Clin Oncol 25: 606-11, 2002.

17) Hall WA, Djalilian HR, Sperduto PW, et al: Stereotactic radiosurgery for recurrent malignant gliomas. J Clin Oncol 13: 1642-8, 1995.

18) Combs SE, Gutwein S, Thilmann C, et al: Stereotactically guided fractionated re-irradiation in recurrent glioblastoma multiforme. J Neurooncol 74: 167-71, 2005.

19) Patel M, Siddiqui F, Jin JY, et al: Salvage reirradiation for recurrent glioblastoma with radiosurgery: radiographic response and improved survival. J Neurooncol 92: 185-91, 2009.

Clinical results of boron neutron capture therapy on previously irrediated patients with recurrent malignant glioma

Shinji Kawabata[1], Ryo Hiramatsu[1], Motomasa Furuse[1], Yoko Matsushita[1], Gen Futamura[1], Hiroyuki Onishi[1], Toshihiko Kuroiwa[1], Natsuko Kondo[2], Minoru Suzuki[2], Yoshinori Sakurai[2], Hiroki Tanaka[2], Koji Ono[2] and Shin-Ichi Miyatake[1]

[1]Department of Neurosurgery, Osaka Medical College, Takatsuki, Osaka, Japan, [2]Kyoto University Reserch Reactor Institute, Kumatori, Osaka, Japan

Abstract: We have applied tumor selective particle irradiation known as boron neutron capture therapy (BNCT) using the nuclear reaction (^{10}B[n, alpha]^{7}Li) to recurrent malignant gliomas (MGs).

We have treated 34 cases of previously irradiated recurrent MGs with BNCT. As there has been no standard treatment for recurrent MGs so far, it has been difficult to evaluate the results of BNCT. Here we introduce the survival benefit of BNCT for recurrent MGs with RPA classification (NABTT, *J Clin Oncol.* 2007).

The median overall survival (OS) was 11.2 (8.9-12.4) months. In the subgroup considered to be a poor prognosis, OS was satisfactory with 11.0 (7.8-11.6) months (*v.s.* 4.4 (3.6-5.4)). The prognostic factor in our experienced cases did not become the tumor size which was on-site histology, steroids / temozolomide history, tumor location (right < left) with the risk.

Earlier BNCT did not become received widely by a problem to use a nuclear reactor as a neutron source. In late years, a technical problem was solved, and clinical trials using the accelerator based BNCT device have been started. In this report, the treatment result with good clinical results of reactor based BNCT for a similar target cases were shown.

key words: glioma, boron neutron capture therapy, recurrence, reirradiation

Miyata et al. Radiation Oncology 2014, 9:51
http://www.ro-journal.com/content/9/1/51

RADIATION ONCOLOGY

RESEARCH Open Access

The roles of platelet-derived growth factors and their receptors in brain radiation necrosis

Tomo Miyata[1], Taichiro Toho[1], Naosuke Nonoguchi[1], Motomasa Furuse[1], Hiroko Kuwabara[2], Erina Yoritsune[1], Shinji Kawabata[1], Toshihiko Kuroiwa[1] and Shin-Ichi Miyatake[1*]

Abstract

Background: Brain radiation necrosis (RN) occurring after radiotherapy is a serious complication. We and others have performed several treatments for RN, using anticoagulants, corticosteroids, surgical resection and bevacizumab. However, the mechanisms underlying RN have not yet been completely elucidated. For more than a decade, platelet-derived growth factors (PDGFs) and their receptors (PDGFRs) have been extensively studied in many biological processes. These proteins influence a wide range of biological responses and participate in many normal and pathological conditions. In this study, we demonstrated that PDGF isoforms (PDGF-A, B, C, and D) and PDGFRs (PDGFR-α and β) are involved in the pathogenesis of human brain RN. We speculated on their roles, with a focus on their potential involvement in angiogenesis and inflammation in RN.

Methods: Seven surgical specimens of RN, obtained from 2006 to 2013 at our department, were subjected to histopathological analyses and stained with hematoxylin and eosin. We qualitatively analyzed the protein expression of each isoform of PDGF by immunohistochemistry. We also examined their expression with double immunofluorescence.

Results: All PDGFs were expressed in macrophages, microglia, and endothelial cells in the boundary of the core of RN, namely, the perinecrotic area (PN), as well as in undamaged brain tissue (UB). PDGF-C, D and PDGFR-α were also expressed in reactive astrocytes in PN. PDGFs and PDGFR-α were scarcely detected in UB, but PDGFR-β was specifically expressed in endothelial cells not only in PN but also in UB.

Conclusions: PDGFs/PDGFRs play critical roles in angiogenesis and possibly in inflammation, and they contribute to the pathogenesis of RN, irrespective of the original tumor pathology and applied radiation modality. Treatments for the inhibition of PDGF-C, PDGF-D, and PDGFR-α may provide new approaches for the treatment of RN induced by common radiation therapies.

Keywords: Angiogenesis, Brain radiation necrosis, Inflammation, Platelet-derived growth factors, Platelet-derived growth factor receptors

Background

Higher radiation doses to tumors result in good local tumor control and improvement in overall survival. On the other hand, radiation necrosis (RN) in the brain occurring after radiotherapy for brain tumors as well as for head and neck cancers is a serious complication that decreases the quality of life in patients. The mechanisms underlying RN have not been completely elucidated. In a previous study we showed that RN specimens stained with hematoxylin and eosin (H&E) typically show marked angiogenesis, so-called telangiectasis, microbleeding, and interstitial edema, probably caused by leakage of plasma from leaky angiogenesis into the surrounding necrotic core—namely, the perinecrotic area (PN) [1].

We and others have applied several treatments for RN, such as anticoagulants, vitamin E, corticosteroids, and surgical resection [2-4]. The typical MRI of symptomatic RN from case 3 demonstrated rapid shrinkage of the perilesional edema after surgical treatment [see Additional file 1 and Table 1]. After surgical resection for the only

* Correspondence: neu070@poh.osaka-med.ac.jp
[1]Department of Neurosurgery, Osaka Medical College, 2-7 Daigaku-machi, Takatsuki City, Osaka 569-8686, Japan
Full list of author information is available at the end of the article

Table 1 Clinical features of patients with symptomatic radiation necrosis

Pt.	Age (y)	Sex	Original dis.	Radiation[a]	Resection area (lobe)	Duration[b]	Chemo
1	46	F	SCC.	XRT (60 Gy), BNCT (13.9 Gy-Eq)	Temporal	7	MTX
2	78	M	Sal. Duc. Ca.	XRT (60 Gy), BNCT (13.9 Gy-Eq)	Frontotemporal	20	-
3	18	M	GBM	XRT (IMRT) (74 Gy)	Parietal	37	-
4	63	F	GBM	XRT (24 Gy), BNCT (13 Gy-Eq)	Frontoparietal	4	-
5	34	M	GBM	XRT (24 Gy), BNCT (13 Gy-Eq)	Frontal	6	-
6	56	F	GBM	Proton + XRT (total 90 Gy)	Temporoparietal	10	ACNU
7	46	F	Ade. Ca.	XRT (30 Gy), SRS (55 Gy, 65 Gy)	Frontal	32	Herceptin

Pt, patient; *y,* year; *F,* female; *M,* male; *Original dis,* original disease; *SCC,* Squamous cell carcinoma; *Sal. Duc. Ca,* salivary ductal carcinoma; *GBM,* glioblastoma; *Ade. Ca,* adenocarcinoma; *XRT,* X-ray radiation treatment; *IMRT* ,intensity modulated radiation therapy; *BNCT,* boron neutron capture therapy; *Proton,* proton beam therapy; *MTX,* methotrexate; *ACNU,* nimustin; *Herceptin,* trastuzumab;
[a]In Pt. 1 and 2, the temporal lobe was included in the irradiation field and in Pt. 3, 4, 5, and 6, local radiation therapy was administered. Pt. 7 had received whole brain irradiation and received SRS twice. In BNCT, the presented dose is the peak point dose for the normal brain.
[b]Months between termination of the last radiotherapy and onset of symptoms caused by radiation necrosis.

enhanced lesion, the perilesional edema decreased rapidly compared with preoperative MRI. This rapid shrinkage of the perilesional edema after surgical treatment was also observed in other cases. In addition, bevacizumab, an antibody for vascular endothelial growth factor (VEGF), has recently shown promising effects on symptomatic brain RN and symptomatic pseudo-progression [5,6]. However, in some cases, treatment with bevacizumab was not sufficient to resolve RN. Some RN cases recurred as RN even after temporary remission by bevacizumab treatment [7].

Recent experiments have shown that demyelination and damage of the normal vasculatures and the appearance of abnormal vasculatures around necrotic foci are major issues in the development of RN [8,9]. In addition, we previously reported that hypoxia-inducible factor 1α (HIF-1α) and VEGF are key molecules in RN [1]. In a later study, we tried to determine whether not only HIF-1α and VEGF, but also proinflammatory cytokines such as IL-1α, IL-6, TNF-α, and NFκB, might play significant roles in RN, since these cytokines were produced by CD68- and hGLUT5-positive microglia and/or macrophages accumulated in PN (in submission).

The platelet-derived growth factors (PDGFs) signaling pathway, which has been extensively studied and shown to play critical roles in many biological processes, is mediated through tyrosine kinase receptors (PDGFR-α, PDGFR-β) [10,11]. There are five members of the PDGF family: PDGF-A, B, and AB, and the recently discovered PDGF-C and D. So far, no heterodimers involving the PDGF-C and D chains have been described. PDGF-A binds only PDGFR-α, whereas PDGF-B activates PDGFR-α, αβ, and β. PDGF-A, B, and C activate PDGFR-α and αβ, while PDGF-D specifically binds to and activates its cognate receptor PDGFR-β. In other words, according to published data, PDGFR-α binds PDGF-A, B, AB, and C, whereas PDGFR-β binds PDGF-B and D [10,12,13].

In addition, PDGF-A and B are secreted in their active forms, while PDGF-C and D are secreted as inactive forms requiring activation for their function [14]. Interestingly, several reports have shown that the structure and biological function of PDGFs are quite similar to those of VEGF [15]. Therefore, the PDGF family is sometimes referred to as the VEGF family. Nevertheless, in recent years it was revealed that the angiogenic pathway induced by PDGF-C is, in large part, VEGF-independent [16].

Based on these findings, in this retrospective study we performed histopathological and immunohistochemical analyses on 7 human RN specimens from patients who we had treated surgically from 2006 to 2013 at our department. We here describe the findings common to all 7 of these specimens, and demonstrate which type of cells produce PDGFs and which type express the PDGFRs. We also evaluated the roles of PDGFs/PDGFRs in brain RN.

Methods

Case selection

Seven surgical specimens, obtained from 2006 to 2013, were submitted for histopathological analysis, staining with H&E, and immunohistochemistry. All the patients had received radiotherapy, including X-ray treatment (XRT), stereotactic radiosurgery (SRS), proton beam therapy, and boron neutron capture therapy (BNCT). The primary diseases were 4 glioblastomas, 2 head and neck cancers, and 1 metastatic brain tumor derived from breast cancer.

In this study we selected the area as radiation necrosis with extensive necrotic area with the boundary of extensive angiogenesis and edema, which is continuous to undamaged brain tissue, as mentioned in Background.

For the 2 patients with head and neck cancers, radiotherapy was used to treat the parotid lesions and the temporal lobe was included in the irradiation field. Therefore, there were no tumor cells in the brain, indicating pure brain RN. The patient characteristics are detailed in Table 1.

Histological and immunohistochemical staining

Histological and immunohistochemical analyses were performed on paraffin sections in which we observed the presence of RN by H&E staining. Each section was immunostained with the following antibodies: PDGF-A (1:20; R&D Systems, USA), PDGF-B (1:20; Abcam, Japan), PDGF-C (1:100; R&D Systems), PDGF-D (1:50; R&D Systems), PDGFR-α (1:20; R&D Systems), and PDGFR-β (1:50; R&D Systems) (Table 2). We routinely use a pressure cooker for 4 minutes to retrieve all the antigens. Endogenous peroxidase was blocked with 0.03% hydrogen peroxide for 40 minutes at room temperature. We used the ABC technique (Vector Laboratories, USA) for all of these antigens, before DAB (3, 3′ diaminobenzidine tetrahydrochloride (Wako Pure Chemical Industries, Japan)). The sections were counterstained with hematoxylin 3G (Sakura Finetek, Japan) and mounted.

Immunofluorescence

Double immunofluorescence was performed using the following antibody combinations: PDGF-C and GFAP (1:25; Dako, Denmark), CD68 (1:25; Epitomics, USA), hGLUT5 (1:50; IBL, Japan), or CD45 (1:50; Epitomics); PDGF-D and GFAP, CD68, hFLUT5, or CD45; PDGFR-α and GFAP, CD68, hGLUT5, or CD31 (1:20; Dako, Denmark); and PDGFR-β and GFAP, CD68, hGLUT5, or CD31.

GFAP, CD68, hGLUT5, CD45, and CD31 were adopted as markers for astrocytes, monocytes, microglia, lymphocytes, and endothelial cells, respectively. All sections were incubated with their respective antibodies for 24 hours with CD68, hGLUT5, and GFAP, and for 48 hours with PDGF-A, B, C, D, and PDGFR-α and β. Then, after washing the primary antibodies, Alexa Fluor 488 (1:25; Molecular Probes, USA) or Alexa Fluor 546 (1:25; Molecular Probes) was used (Table 3). Finally, the sections were examined using an LSM510 laser scanning confocal microscope (Carl Zeiss, Germany).

Table 2 List of primary antibodies used

Antibody	Clone	Sources	Type	Dilution
PDGF-A		R&D Systems, Minneapolis, MN	p/g	1:20
PDGF-B	MM0014-5 F66	Abcam Cambridge, MA	m/m	1:20
PDGF-C		R&D Systems, Minneapolis, MN	p/g	1:100
PDGF-D		R&D Systems, Minneapolis, MN	p/g	1:50
PDGFR-α		R&D Systems, Minneapolis, MN	p/g	1:20
PDGFR-β		R&D Systems, Minneapolis, MN	p/g	1:50
CD68	KP-1	Dako, Glostrup, Denmark	m/m	1:25
hGLUT5		IBL, Tokyo, Japan	p/r	1:50
GFAP	6 F2	Dako, Glostrup, Denmark	m/m	1:25
CD45	EP322Y	Eptomics, Burlingame, CA	m/r	1:50
CD31	JC70A	Dako, Glostrup, Denmark	m/m	1:20

p/g polyclonal goat; *p/r*, polyclonal rabbit; *m/r*, monoclonal rabbit; *m/m*, monoclonal mouse.

Statistical analysis

We assessed the frequency of expression of PDGFs semi-quantitatively by the following method. Five fields of each PDGF isoform in which abnormal angiogenesis was detected were randomly selected with a microscope. PDGF-positive mononuclear cells were counted. We observed 7 cases and, to reduce bias, used two observers to count the cells. One observer, who was blinded to the patients' clinical and pathological information, evaluated the results of immunohistochemical staining. The ratios of PDGF-positive cells per total cells in each field were calculated, and we statistically analyzed the data with Steel-Dwass tests using JMP Pro 10 (SAS Institute, USA). The results revealed that PDGF-C and D showed higher frequency of expression than PDGF-A and B in PN. The difference was statistically significant.

Ethical approval

This study was approved by an institutional committee of Osaka Medical College. The research was in compliance with the Helsinki Declaration.

Results

Expression of PDGFs

Figure 1 shows the results of H&E staining and immunohistochemistry from case 1. H&E staining revealed a necrotic

Table 3 Double immunofluorescence combinations

Primary	Dilution	Secondary	Primary	Dilution	Secondary
PDGF-C	1:50	F488	CD68	1:25	F546
PDGF-C	1:50	F488	hGLUT5	1:50	F546
PDGF-C	1:50	F488	GFAP	1:25	F546
PDGF-C	1:50	F488	CD45	1:50	F546
PDGF-D	1:20	F488	CD68	1:25	F546
PDGF-D	1:20	F488	hGLUT5	1:50	F546
PDGF-D	1:20	F488	GFAP	1:25	F546
PDGF-D	1:20	F488	CD45	1:50	F546
PDGFR-α	1:10	F488	CD68	1:25	F546
PDGFR-α	1:10	F488	hGLUT5	1:50	F546
PDGFR-α	1:10	F488	GFAP	1:25	F546
PDGFR-α	1:10	F488	CD31	1:20	F546
PDGFR-β	1:20	F488	CD68	1:25	F546
PDGFR-β	1:20	F488	hGLUT5	1:50	F546
PDGFR-β	1:20	F488	GFAP	1:25	F546
PDGFR-β	1:20	F488	CD31	1:20	F546

Primary, primary antibody; *Secondary*, secondary antibody; *F488*, Alexa Fluor 488; *F546*, Alexa Fluor 546.

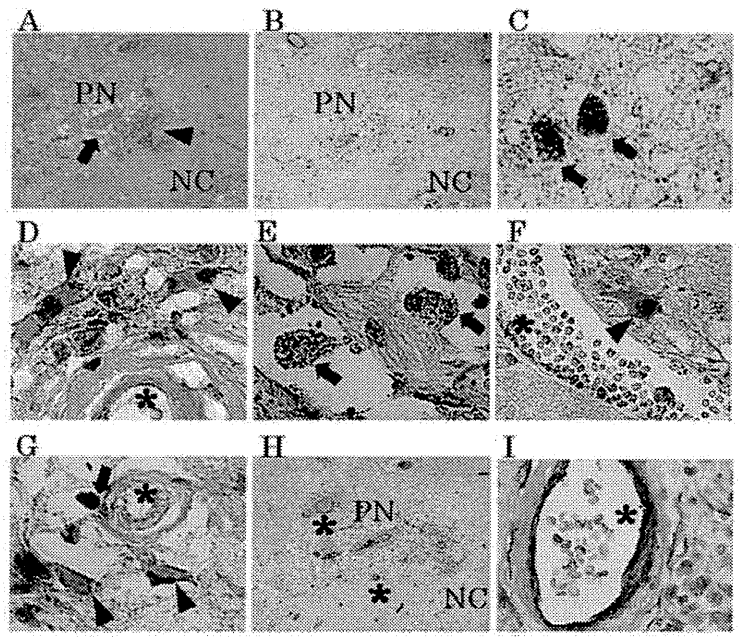

Figure 1 Results of hematoxylin and eosin staining (H&E) and immunohistochemistry from case 1. H&E staining **(A)** revealed a necrotic core (NC) and perinecrotic area (PN), including micro bleeding (**A**, arrowhead) and abnormal angiogenesis (**A**, arrow). Immunostaining results for PDGF-C are presented as a representative example **(B)**. PDGF-C **(C and D)**, D **(E and F)** and PDGFR-α **(G)** were produced by monocytic cells (**C, E, G**, arrow) and reactive astrocytic cells (**D, F, G**, arrowhead) in PN. On the other hand, PDGFR-β **(H and I)** was expressed mainly in endothelial cells **(H and I*)**. There was partially nonspecific staining in NC **(B)** or around blood vessels **(I)**. Original magnification, **A, B** and **H** × 40, **C, D, E, F, G** and **I** × 200.

core (NC) (Figure 1A. NC) and PN (Figure 1A. PN), in which micro bleeding (Figure 1A. arrowhead) and abnormal angiogenesis (Figure 1A. arrow) were confirmed. PDGF-A, B, C, and D-positive cells were detected in PN. The results of immunostaining for PDGF-C are shown as a typical example of these distribution analyses (Figure 1B, C, D). Morphologically, PDGF-A and B were produced by some monocytic cells [see Additional file 2] in PN. On the other hand, PDGF-C and D (Figure 1E, F) were produced by many monocytic cells (arrows in Figure 1C, E), reactive astrocytic cells (arrowheads in Figure 1D, F), and endothelial cells (Figure 1D*). PDGF-A, B, C, and D were scarcely detectable in UB (Figure 2).

These relationships among the expression of PDGFs are summarized in Table 4. These relationships were also confirmed with other specimens [see Additional file 3].

Our statistical analysis revealed that PDGF-C and D showed higher frequencies of expression than PDGF-A and B in PN. The difference was statistically significant ($p < 0.0001$, Steel-Dwass test) (Figure 3). We also grouped the cases into a GBM group (cases 3, 4, 5, 6) and non-GBM group (cases 1, 2, 7) and analyzed the differences in protein expression between them. No statistically significant differences in the expression of any of the isoforms were observed between the two groups by the Steel-Dwass test [see Additional file 4]. Therefore, we considered that these primary diseases did not affect the expression of PDGFs.

Double immunofluorescence from case 1 revealed that PDGF-C or D-positive cells were merged with many cells positive for CD68 (Figure 4A, E), GFAP (Figure 4B, F), hGLUT5 (Figure 4C, G), and CD45 (Figure 4D, H).

H&E staining, immunohistochemistry, and double immunofluorescence also showed similar tendencies in other specimens with symptomatic RN [see Additional files 3, and 5].

Expression of PDGFRs

PDGFR-α was expressed in endothelial cells (Figure 1G*), monocytic cells (Figure 1G arrow), and reactive astrocytic cells (Figure 1G, arrowhead) in PN. PDGFR-β was expressed mainly in endothelial cells (Figure 1H, I*). PDGFR-α was not expressed in any types of cells in UB (Figure 2E), but PDGFR-β was detected in endothelial cells in both PN and UB (Figure 2F).

Double immunofluorescence revealed that PDGFR-α and β were strongly expressed in CD31-positive cells (Figure 5D, I). PDGFR-β-positive cells were merged specifically with endothelial cells (Figure 5F, G, H, I and J, *), but PDGFR-α-positive cells were merged with cells positive for CD68 (Figure 5A), GFAP (Figure 5B), hGLUT5 (Figure 5C), and CD45 (Figure 5E) in PN.

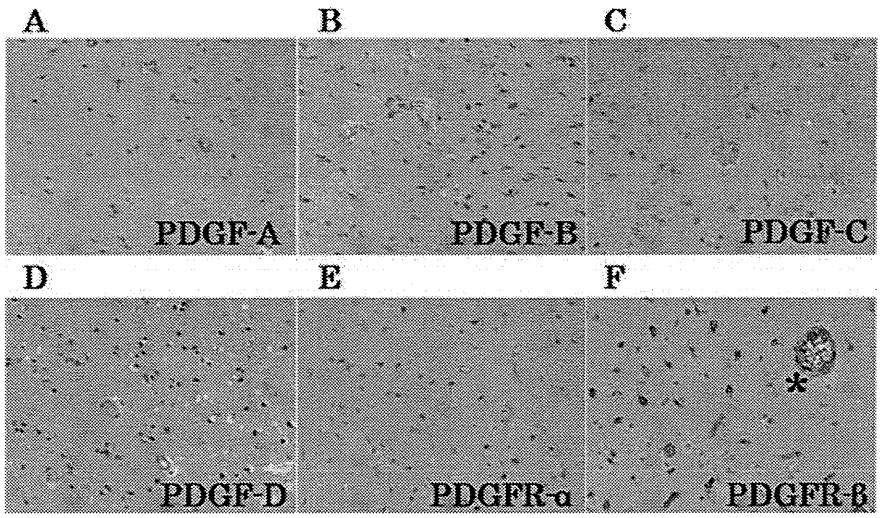

Figure 2 Representative results of immunostaining of undamaged brain tissue (UB). PDGF-**A, B, C, D** and PDGFR-α were scarcely detectable in UB **(A through E)**. PDGFR-β **(F)** was specifically expressed in endothelial cells in UB. Many normal cerebral blood vessels stained with PDGFR-β **(F *)** were detected in UB. Original magnification, ×200.

These findings from case 1 were confirmed in other specimens with symptomatic RN [see Additional file 6].

Double immunofluorescence revealed partially non-specific staining, especially in endothelial cells (Figures 4, and 5*). In cases where immunofluorescence was performed with GFAP alone, vascular endothelial cells were not stained [see Additional file 7]. These findings were also observed in other specimens.

Discussion

PDGFs are a group of multifunctional proteins with a wide variety of effects. They have important physiologic functions in embryonic and organ development, have been implicated in a wide variety of pathological processes, including proliferation, differentiation, and fibrogenesis, and are essential for the stability of normal blood vessel formation [16-19]. However, the overexpression of

Table 4 Expression of PDGFs/PDGFRs in two areas of the brain

	UB			PN		
	Mono	Astro	Endo	Mono	Astro	Endo
PDGF-A	-	-	-	+	-	+
PDGF-B	-	-	-	+	-	+
PDGF-C	-	-	-	+	+	+
PDGF-D	-	-	-	+	+	+
PDGFR-α	-	-	-	+	+	+
PDGFR-β	-	-	+	-	-	+

UB, undamaged brain area; *PN*, perinecrotic area; *Mono*, monocytes, including macrophages, microglia and lymphocytes *Astro*, reactive astrocytes; *Endo*, endothelial cells ; -, not expressed; +, expressed.

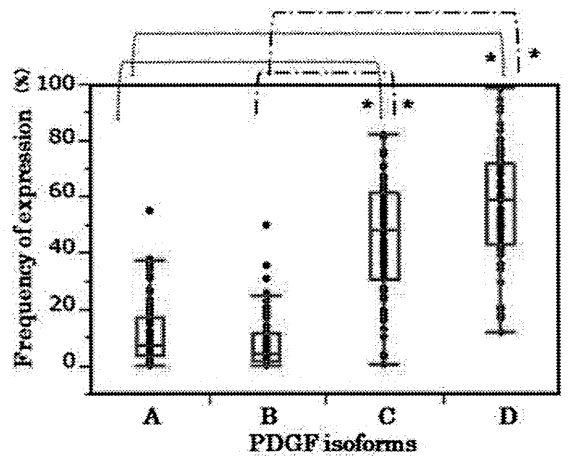

Figure 3 Frequency of expression. We assessed the frequency of expression of PDGFs semi-quantitatively by the following method. Five fields of each PDGF isoform, in which abnormal angiogenesis were detected, were randomly selected with a microscope. The PDGF-positive mononuclear cells were counted. We observed all 7 cases and performed the counting using two observers to reduce bias. One observer, who was blind to the patients' clinical and pathological information, evaluated the results of the immunohistochemical staining. The ratios of PDGF-positive cells to total cells in each field were calculated and were statistically analyzed using Steel-Dwass tests with JMP Pro 10 (SAS Institute Inc, Cary, NC, USA). Statistical analysis revealed that PDGF-C and D showed higher frequency of expression in the PN specimens than did PDGF-A and B. The difference was statistically significant (*$p < 0.0001$, Steel-Dwass test).

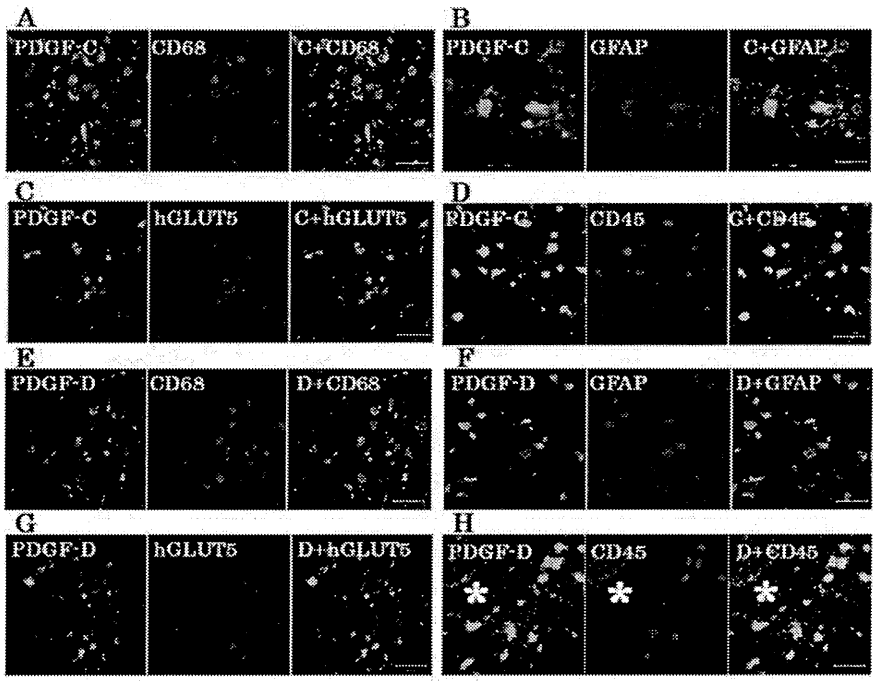

Figure 4 Double immunofluorescence staining. The results of double immunofluorescence staining from case 1 revealed that PDGF-C or D-positive cells were merged with many CD68 **(A, E)**, GFAP **(B, F)**, hGLUT5 **(C, G)**, and CD45 **(D, H)** -positive cells in PN. Some PDGF-C or D-positive cells did not express CD68, GFAP, hGLUT5 or CD45 and vice versa. Endothelial cells **(*)** were nonspecifically stained with secondary fluorescence antibody. The scale bar represents 50 μm.

PDGFs has adverse effects. Previous studies also have demonstrated that various cell types, including macrophages, fibroblasts, pericytes, and capillary endothelial cells, express PDGFs [20,21]. Deuel et al. also reported that a macrophage-derived PDGF induces chemotaxis and the proliferation of monocytes and fibroblasts during inflammation and wound repair [22].

This is the first study to explore the expression of PDGF isoforms and PDGFRs in human brain RN. Our results have shown that all PDGFs and PDGFRs were expressed in brain RN, and that PDGFs and PDGFRα were primarily expressed by macrophages, microglia, reactive astrocytes, lymphocytes, and endothelial cells in PN. These findings suggest that the activation of PDGFs is coincident with inflammation, angiogenesis, and fibrogenesis in the pathophysiology of RN.

Our recent study revealed that CD45-positive lymphocytes expressing CXCR4 might be drawn into PN from peripheral blood by chemotaxis, but they do not express proinflammatory cytokines, and their roles in RN remain unclear (submitted for publication). However, in the present study, CD45-positive lymphocytes produced PDGF-C and -D. These results suggest that CD45-positive lymphocytes in PN do not produce proinflammatory cytokines but may play significant indirect roles in angiogenesis and/or inflammation.

The highest differences of expression among PDGFs on brain RN were observed in PDGF-C and D (Figure 3 and Additional file 4). In this study, the expressions of PDGF-C and D were significantly higher than the expressions of PDGF-A and B in PN. Our current immunohistochemical study has further revealed that inflammatory cells, including macrophages, microglia, and even lymphocytes, were gathered in PN and produced PDGF-C and D. These mononuclear cells are known to play important roles in wound healing and inflammatory disease by producing a variety of growth factors and cytokines [23,24]. In our recent study, these mononuclear cells produced inflammatory cytokines (IL-1α, IL-6, TNF-α, NFκB) (submitted for publication). In the present study, these cells also produced PDGF-C and D. Therefore the activation of PDGF-C and D is coincident with inflammation as well as angiogenesis. These findings suggest that PDGF-C and D are involved in multiple aspects of brain RN.

The present and previous reports have revealed that the differential expression of PDGFs has also been seen in pathological conditions other than RN. In the aortic ring outgrowth assay, PDGF-C mediated significantly increased outgrowth, comparable to the levels mediated by VEGF and PDGF-A and B [25]. The angiogenic activity of PDGF-C in vivo is more potent than that of PDGF-A, AB or B [26]. PDGF-D also has been shown to stimulate